Design and Evaluation of a Zero Mass Flow Liner

Ralf Burgmayer [†]
German Aerospace Center (DLR), 10623, Berlin, Germany

Friedrich Bake[‡]
Bundesanstalt für Materialforschung und -prüfung (BAM), Berlin, 12205, Germany

Lars Enghardt[§]
German Aerospace Center (DLR), 10623, Berlin, Germany

In this study, the concept of a Zero Mass Flow Liner is evaluated. The concept enables impedance control by the induction of, acoustically actuated, periodic bias flow through the facing sheet of the liner. By means of the periodic bias flow, the impedance of the liner is adapted to different grazing flow conditions. The equivalent fluid impedance model for perforated plates is modified to account for the effects of periodic bias and grazing flow. A generally applicable optimization routine, using the impedance of the lined surface as a boundary condition in a numeric calculation, is implemented. Based on the results of the optimization, a Zero Mass Flow Liner is manufactured and evaluated experimentally. The damping characteristics are assessed in form of the dissipated energy along the lined surface. Prediction and measurements show reasonable agreement. The Zero Mass Flow Liner delivers broadband dissipation of high peak value over a range of grazing flow Mach numbers. Under grazing flow, the effect of periodic bias flow is reduced. For a ratio of grazing to bias flow velocities larger than five, no appreciable effect is found. This poses considerable energy requirements on the actuation source for the application in high Mach number flow regimes.

Nomenclature

c_0	=	Speed of sound in air [m s^{-1}]
$C_{d,nl}$	=	Empirical discharge coefficient accounting for periodic bias flow effects
d	=	Orifice diameter [m]
D_{cav}	=	Cavity depth [m]
D	=	Length of perfectly matched layer (PML) in x-direction [m]

Presented as Paper 2022-2820 at the 28th AIAA/CEAS Aeroacoustics 2022 Conference, June 14-17, Southampton, United Kingdom
[†]Research Assosciate, DLR Institute of Propulsion Technology, Engine Acoustics, ralf.burgmayer@dlr.de.
[‡]Head of the Division for Acoustic and Electromagnetic Methods, BAM, AIAA Senior Member, friedrich.bake@bam.de.
[§]Professor, DLR Institute of Propulsion Technology, Engine Acoustics, AIAA Member, lars.enghardt@dlr.de.

f_p	=	Frequency of the primary excitation (sound field in the main duct) [Hz]
f_s	=	Frequency of the secondary excitation (periodic bias flow) [Hz]
h	=	Thickness of the perforated facing sheet [m]
k	=	Turbulence intensity constant
k_p	=	Axial wave number of the primary excitation [m^{-1}]
L_{eff}	=	Effective length of the lined surface [m]
l_{GF}	=	Change of end correction due to grazing flow
l_s	=	Change of end correction due to secondary actuation (periodic bias flow)
M_{avg}	=	Average (bulk) grazing flow mach number
p	=	Acoustic pressure of the primary excitation (sound field in the main duct) [Pa]
p_s	=	Acoustic pressure of the secondary excitation (periodic bias flow) [Pa]
r	=	Orifice radius [m]
St_p	=	Periodic bias flow Strouhal number
u_s	=	Acoustic particle velocity in the orifices of the facing sheet, induced by the secondary actuation (periodic bias flow) [m
v_{avg}	=	Average (bulk) grazing flow velocity [$\mathrm{m\,s}^{-1}$]
α_∞	=	Tortuosity
δ	=	Inertial end correction
ζ	=	Specific impedance of the perforated plate
ζ_{Cav}	=	Specific impedance of the cavity
ζ_{exit}	=	Specific impedance at the exit of the numerical domain
ζ_{ZML}	=	Specific impedance of the Zero Mass Flow Liner
$Re\{\Delta\zeta_s\}$	=	Resistance due to secondary actuation (periodic bias flow)
$Re\{\Delta\zeta_{GF}\}$	=	Resistance due to grazing flow
η	=	Dynamic viscosity [$\mathrm{kg\,m}^{-1}\,\mathrm{s}^{-1}$]
Λ	=	Hydraulic radius [m]
ρ_0	=	Density of air [$\mathrm{kg\,m}^{-3}$]
$\tilde{\rho}_e$	=	Effective density [$\mathrm{kg\,m}^{-3}$]
σ	=	Flow resistivity [$\mathrm{kg\,m}^{-3}\,\mathrm{s}^{-1}$]
τ	=	Cost function
Φ	=	Porosity of the facing sheet
ψ	=	Correction for hole interaction
ω_p	=	Angular frequency of the primary excitation (sound field in the main duct) [s^{-1}]

I. Introduction

Increased noise regulations in aviation necessitate liner concepts with improved low frequency and broadband damping. In 2008, Heuwinkel et al. [1] presented the concept of a so-called Zero Mass Flow Liner, where an acoustic actuator is attached to the cavity of a Helmholtz resonator liner, emitting a secondary high amplitude sound field and inducing periodic bias flow in the orifices of the facing sheet. The periodic bias flow causes flow separation at the orifices of the facing sheet, enabling control of the impedance by adjusting the amplitude of the periodic bias flow. Thereby, the net mass flow through the facing sheet of the liner is zero. Lahiri et al. [2] described the design of an aeroacoustic actuator as source for the excitation of periodic bias flow. This configuration requires some air supply, but reduces the mass flow rate by 60 % at similar performance when compared to a conventional steady bias flow liner. While demonstrating extended dissipation characteristics, dependent on the actuation strength, no quantitative analysis of the underlying physics has been conducted. Based on dimensional analysis, the effects of a secondary high amplitude stimulus, i.e. periodic bias flow, on the impedance of a perforated plate at primary sound field frequencies have been analyzed experimentally. The secondary and primary stimuli were unrelated in terms of frequency and phase. A semi-empirical model describing the change of impedance is deduced from the measurements. [3, 4]

This manuscript describes the design and the consecutive experimental evaluation of a Zero Mass Flow Liner. The process is decomposed into three steps: First, the equivalent fluid impedance model, derived by Atalla and Sgard [5], is modified to account for the effects due to secondary periodic bias flow and grazing flow [3, 4, 6]. Second, an optimization routine, based on a numerical simulation and a genetic algorithm [7], is implemented. The optimization routine serves the purpose of deriving a set of geometric liner parameters and the required secondary periodic bias flow actuation to maintain a dissipation of broadband characteristic and high peak value over a range of grazing flow velocities. In the process, the two dimensional Helmholtz Equation is solved numerically to calculate the sound pressure distribution in a duct with mean flow. Thereby, the impedance calculated from the derived impedance model, is used as boundary condition in the simulation, making the method applicable to arbitrary lined surfaces. From the sound pressure distribution in the duct, the dissipation characteristics of the lined surface are determined. The difference between the calculated dissipation and a target dissipation is minimized by the iterative variation of the geometric parameters of the liner and the strength of the periodic bias flow. Using the parameters obtained in the optimization process, a liner is manufactured. To maintain flexibility regarding the actuation frequency of the periodic bias flow, loudspeakers are used for excitation. Third, the manufactured Zero Mass Flow Liner is evaluated experimentally. The measured dissipation is compared to the results of the simulation for grazing flows up to average Mach numbers of 0.2. The combination of periodic bias and grazing flow is studied and the experimental results are discussed with respect to the applicability of the Zero Mass Flow concept.

II. Zero Mass Flow Concept

Figure 1 depicts a schematic of the Zero Mass Flow Liner (ZML). An acoustic actuator, emitting high amplitude sound waves, is attached to the cavity of a Helmholtz resonator liner. In general, any form of acoustic source able to emit high amplitude signals can be used. Lahiri et al., for example, used an aeroacoustic actuator. The aeroacoustic actuation relies on the production of an edge tone by applying mass flow to a simple and robust jet-edge configuration. The frequency and sound pressure level can be tuned by adjustment of the edge distance and the mass flow rate [2]. For the sake of increased flexibility, in this study, loudspeakers are used. Due to the high amplitude sound wave emitted by the actuator, periodic bias flow is induced in the orifices of the facing sheet, leading to flow separation and altering the impedance of the liner and consequently affecting its damping characteristics. The periodic bias flow, referred to as secondary flow, is quantified by the amplitude of the root mean squared (RMS) particle velocity in the orifices of the perforated facing sheet $|\bar{u}_s|$. By adjusting $|\bar{u}_s|$, the impedance of the lined surface can thus be adapted to specific operating conditions. With increasing $|\bar{u}_s|$, the real part of the impedance (resistance) increases, while the imaginary part (reactance) decreases. The sound waves in the main duct, traversing the lined surface, are referred to as primary sound field. Primary and secondary sound fields are unrelated in terms of frequency and the phase relation is disregarded.

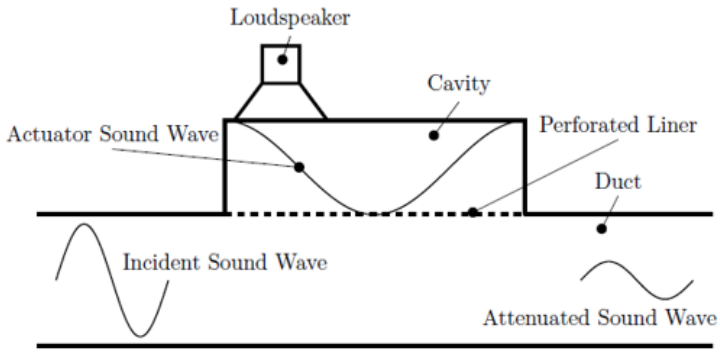

Fig. 1 Schematic of a Zero Mass Flow Liner in a duct configuration. [1]

III. Impedance Model for the Zero Mass Flow Liner under Grazing Flow

Atalla and Sgard use the equivalent fluid approach to derive an impedance model for perforated plates [5]. The model can be applied to macro and micro perforated plates at low sound pressure amplitudes and without grazing flow. At low sound pressure amplitudes, in the so-called linear impedance regime, the impedance is independent of the incident sound pressure. The dependency of the impedance of orifices and perforated plates on high sound pressure amplitudes and, consequently, large particle velocities inside the orifices, is generally referred to as acoustic nonlinearity. [8] In the context of the Zero Mass Flow concept, an additional high sound pressure amplitude actuation is deliberately used to induce flow separation and affect the impedance at frequencies different from the actuation frequency. In the case of a continuous flow grazing the facing sheet of a liner, a turbulent boundary layer is formed at the perforated

plate. The resulting pressure fluctuations superpose the acoustic flow causing an increase of resistance and a decrease of reactance. [9, 10] Following the approach of Laly et al. [11], this section describes the extension of the equivalent fluid model to account for secondary periodic bias and grazing flow. The specific impedance of the perforated plate is given by equation (1):

$$\zeta = j\frac{\omega_p h}{\rho_0 c_0 \Phi}\tilde{\rho}_e, \tag{1}$$

where h represents the plate thickness and $\omega_p = 2\pi f_p$ is the circular frequency. f_p is the frequency of the primary sound field, excited in the main duct. ρ_0 and c_0 represent the density and speed of sound in air and Φ represents the porosity of the perforated plate. $\tilde{\rho}_e$ denotes the effective density given as:

$$\tilde{\rho}_e = \alpha_\infty \rho_0 \left(1 + \frac{\sigma\Phi}{j\omega_p \alpha_\infty \rho_0}\sqrt{1 + \frac{4j\rho_0\omega_p\eta\alpha_\infty^2}{\Phi^2\sigma^2\Lambda^2}}\right), \tag{2}$$

where η represents the dynamic viscosity of air and Λ the hydraulic radius of the orifices. In case of circular orifices, the hydraulic radius is equal to the orifice radius $\Lambda = r$. $\tilde{\rho}_e$ is a function of the flow resistivity σ and the tortuosity α_∞. σ is given by:

$$\sigma = \frac{8\eta}{\Phi r^2} \tag{3}$$

and α_∞ is defined as:

$$\alpha_\infty = 1 + \frac{2\delta\psi}{h}, \tag{4}$$

where $\delta = 0.48\sqrt{\pi r^2}$ represents the one-sided inertial end correction and ψ represents a function to account for the interaction of adjacent orifices. Here, for ψ, we use the derivation of Fok [12].

High sound pressure amplitudes, bias and grazing flows affect the impedance by altering σ and α_∞. The change of resistance due to a high amplitude secondary sound wave, i.e. periodic bias flow is given as:

$$Re\{\Delta\zeta_s\} = \frac{(1-\Phi^2)|\bar{u}_s|}{2c_0\Phi C_{d,nl}^2} \cdot \left(1 - \frac{f_p d}{|\bar{u}_s|}\right), \text{ for } 1/St_{p,d} \geq \frac{1}{2\pi}, \tag{5a}$$

$$Re\{\Delta\zeta_s\} = 0, \text{ for } 1/St_{p,d} < \frac{1}{2\pi}. \tag{5b}$$

The first term on the right hand side of Eq. (5a) accounts for the increase in resistance under quasi-steady flow conditions, where $C_{d,nl}$ describes the discharge coefficient approximated empirically [3]. The second term on the right

hand side, where d represents the diameter of the orifices of the perforated sheet, accounts for deviations from the quasi-steady assumption in the transmission region between linear and quasi-steady flow domains. This correction term is derived from previous measurements in Appendix A. The periodic bias flow Strouhal number, defined as $St_{p,d} = \frac{2\pi f_p d}{|\bar{u}_s|}$, is used to differentiate between linear, transitional and quasi-steady flow regimes. For low $|\bar{u}_s|$, high f_p and large d, the correction term can become negative. Therefore, in case $\frac{f_p d}{|\bar{u}_s|} > 1$, we assume, that the resistance is independent of the secondary particle velocity and $Re\{\Delta\zeta_s\} = 0$. The value of $\frac{f_p d}{|\bar{u}_s|} = 1$ corresponds to an inverse Strouhal number of $1/St_{p,d} = \frac{1}{2\pi} \approx 0.16$ and, thus, to minor effects due to the secondary actuation.

To account for the effects of grazing flow on the resistance, the expression of Guess [6] is used:

$$Re\{\Delta\zeta_{GF}\} = \frac{(1-\Phi^2)}{\Phi} \cdot k \cdot M_{avg}, \tag{6}$$

where k is a measure of the turbulence intensity and is set to $k = 0.3$. M_{avg} depicts the grazing flow Mach number, estimated from the bulk grazing flow velocity v_{avg}, for details refer to Sec.V.A. σ, representing the resistance per unit thickness, is increased due to the secondary periodic actuation and the grazing flow. Using Eqs. (5) and (6), the flow resistivity is expressed as:

$$\sigma_{fs} = \frac{8\eta}{\Phi r^2} + \rho_0 c_0 \frac{(Re\{\Delta\zeta_s\} + Re\{\Delta\zeta_{GF}\})}{h}, \tag{7}$$

where, in a first approximation, an additive relation between the convective terms is used [9, 10].

Grazing flows as well as the periodic bias flow also affect the reactive part of the impedance. The inertial end correction of the perforate and, hence, the tortuosity is reduced. The loss of end correction, induced by the secondary flow, is accounted for by multiplying the end correction with the empirical factor l_s[4]:

$$l_s = 0.38 + \frac{0.68}{1 + 1/St_{p,h}^2}, \tag{8}$$

where $St_{p,h} = \frac{2\pi f_p h}{|\bar{u}_s|}$ is the periodic bias flow Strouhal number based on the plate thickness. Equations (5) and (8), accounting for the change of impedance due to periodic bias flow, were derived and experimentally evaluated for perforated plates with $1\% \leq \Phi \leq 6.18\%$ and $0.75 \leq d/h \leq 2.5$, where d/h represents the ratio of orifice diameter to plate thickness. The reduction of end correction due to grazing flow is accounted for by multiplying the end correction by the approximation of Guess [6]:

$$l_{GF} = \frac{1}{1 + 305 M_{avg}^3}. \tag{9}$$

Consequently, the tortuosity in case of periodic bias flow and grazing flow is rewritten as:

$$\alpha_{\infty,fs} = 1 + \frac{2\delta\psi}{h} \cdot l_s \cdot l_{GF}. \tag{10}$$

Incorporating σ_{fs} and $\alpha_{\infty,fs}$ into Eq. (2), the effective density under periodic bias flow and grazing flow $\tilde{\rho}_{e,fs}$ is written as:

$$\tilde{\rho}_{e,fs} = \alpha_{\infty,fs}\rho_0\left(1 + \frac{\sigma_{fs}\Phi}{j\omega_p\alpha_\infty\rho_0}\sqrt{1 + \frac{4j\rho_0\omega_p\eta\alpha_{\infty,fs}^2}{\Phi^2\sigma^2\Lambda^2}}\right). \tag{11}$$

The cavity is, under the assumption of a rigid back wall and the sole propagation of plane waves, modelled using the common expression $\zeta_{Cav} = -j\cot(\omega_p D_{cav}/c_0)$, where D_{cav} is the cavity depth. Thus, the impedance of the ZML under secondary actuation and grazing flow is:

$$\zeta_{ZML} = j\frac{\omega h}{\rho_0 c_0 \Phi}\tilde{\rho}_{e,fs} - j\cot(\omega_p D_{cav}/c_0). \tag{12}$$

The effects of high amplitude primary sound fields on the impedance are not incorporated since they can be neglected if the particle velocity in the orifices due to the secondary excitation is larger than the orifice velocity induced by the primary excitation [3].

IV. Optimization, Numerical Method, Liner Design and Manufacturing

A. Optimization Method and Assumptions

The goal of the optimization procedure is to derive a set of geometric parameters for the facing sheet of the liner (hole diameter d, plate thickness h and porosity Φ) and appropriate secondary bias flow velocities $|\bar{u}_s|$, that grant dissipation of high peak value and large frequency bandwidth over a range of grazing flow velocities. The procedure is only applied to the case of upstream excitation, i.e. to the case of downstream propagation of the primary sound field. For downstream excitation (i.e. upstream propagation of the primary sound waves), a separate optimization is necessary. The depth of the cavity is set to a fixed value of $D_{cav} = 60$ mm to enable the estimation of the secondary particle velocity in the cavity by a plane wave decomposition during the subsequent experimental evaluation. Note, that the cavity depth is the parameter that mainly defines the resonance frequency of the liner.

A genetic optimization algorithm is applied to the problem [7]. In the course of the optimization, a cost function τ is minimized, based on the difference between a predefined target dissipation curve and the dissipation, calculated within the optimization procedure. The cost function τ is considered to be minimized either after 150 iterations or after ten consecutive iterations without improvement. The resulting parameters, the respective impedance and dissipation characteristics of the lined surface are referred to as optimized. τ is defined as:

$$\tau = 1 - \frac{1}{f_{p,2} - f_{p,1}} \int_{f_{p,1}}^{f_{p,2}} \Delta^{+} df_p, \tag{13}$$

where $f_{p,1}$ and $f_{p,2}$ denote the lower and upper cut-off frequencies and Δ^{+} represents the dissipation in case of upstream excitation. $f_{p,1}$ is set to $f_{p,1}$ = 408 Hz and $f_{p,2}$ is set to $f_{p,2}$ = 1734 Hz respectively. Increasing the frequency band further does not increase the bandwidth of the optimized dissipation curve appreciably. With increasing frequency range, however, the computation time of the optimization procedure increases. Thus, the frequency band is selected as a compromise between the computation time and the gain in dissipation bandwidth.

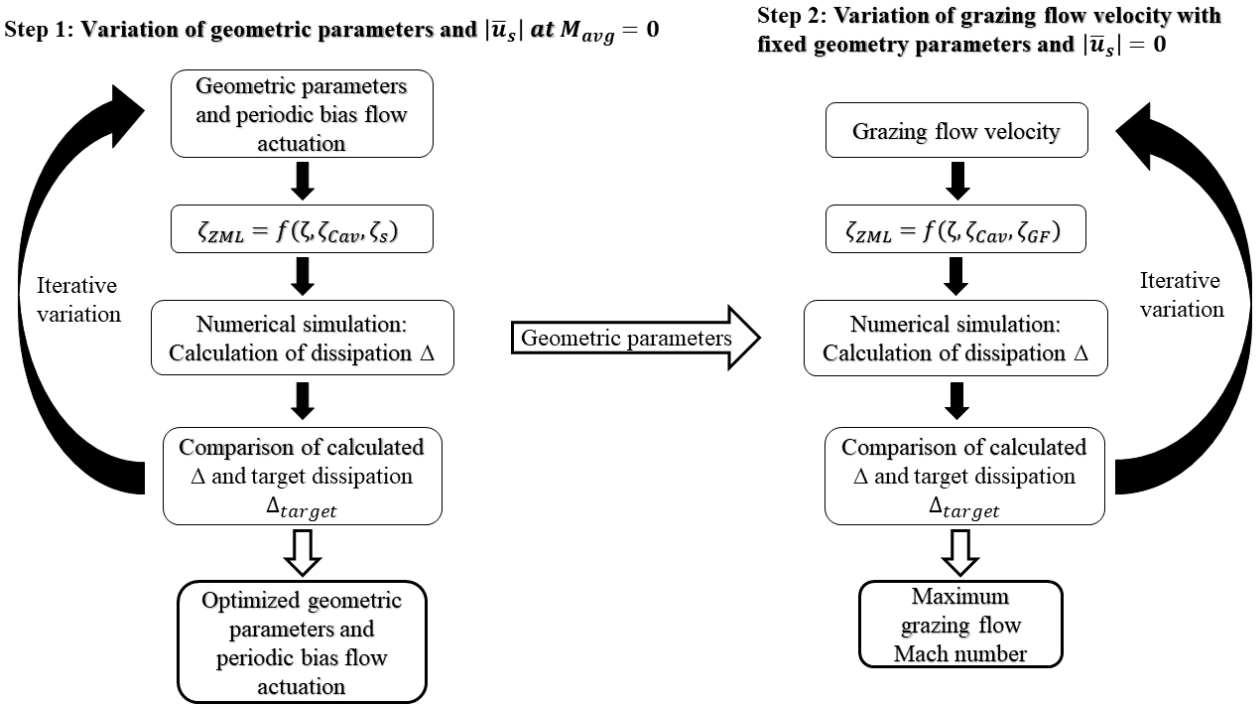

Fig. 2 Flow diagram of the optimization routine.

Fig. 2 depicts a flow chart outlining the optimization process. The process comprises two separate optimizations. In the first step, an optimization is conducted at $M_{avg} = 0$ and $|\bar{u}_s| > 0$ to derive a set of geometric parameters and the correspondingly required periodic bias flow velocity $|\bar{u}_{s,opt}|$ that approximate the desired dissipation characteristics when no grazing flow is present. The optimization is initiated with arbitrary values within the parameter range given in table 1. The impedance of the ZML, calculated via Eq. 12, is used as boundary condition in the numeric calculations, described in Sec. IV.B, and is iteratively varied by changing the geometric parameters of the facing sheet and $|\bar{u}_s|$. For every iteration, the sound propagation, restricted to plane waves, is calculated in the duct. By a plane wave decomposition, the scattering coefficients and the dissipation along the lined section of the duct are calculated. The calculated dissipation is compared to the target dissipation. This process is repeated until τ is minimized. The optimized

geometric parameters of the facing sheet and the respectively required $|\bar{u}_{s,opt}|$ are displayed in line one of table Table 2.

Both, grazing flow and periodic bias flow affect the impedance of the liner in similar ways: The real part of the impedance (resistance) increases, while the imaginary part (reactance) decreases. Accordingly, with increasing grazing flow speeds, the required $|\bar{u}_s|$, to keep the impedance near its optimum value, will decrease. At a certain grazing flow Mach number $M_{avg,opt}$, no periodic bias flow will be required and the impedance of the liner and, consequently, its dissipation characteristics approximate their respective optimum values. $M_{avg,opt}$ represents the maximum grazing flow Mach number up to which the ZML concept can be applied. Focusing on the resistance, at grazing flows with $M_{avg} > M_{avg,opt}$ the resistance of the liner is inevitably too large to achieve the desired dissipation characteristics.

Therefore, to assess the upper limit of the operational capability of the ZML and estimate $M_{avg,opt}$, in the second step, the optimization scheme is reapplied under variation of M_{avg} with the derived geometric properties of step one set to constant and $|\bar{u}_s| = 0$. Hence, τ is minimized by the sole variation of the grazing flow velocity. Without the periodic bias flow actuation active, the ZML acts as a traditional single degree of freedom (SDOF) liner. By adjusting $|\bar{u}_s|$ accordingly, a high degree of dissipation should be provided for $0 \leq M_{avg} \leq M_{avg,opt}$. The maximum grazing flow Mach number $M_{avg,opt}$, derived from the optimization, is displayed in line two of table Table 2.

Table 1 Limiting values for the variation of parameters in the optimization.

Parameter	min	max
$\lvert\bar{u}_s\rvert$ [m/s]	0	15
d [mm]	1	2.5
h [mm]	1	2
d/h	0.75	2.5
Φ [%]	1	6

To have an estimate of the required periodic bias flow velocity at an intermediate grazing flow Mach number smaller than $M_{avg,opt}$, in an optional step, the optimization with fixed geometric parameters and variable $|\bar{u}_s|$ can be applied at the desired Mach number.

Figures 3 a) and b) depict the respective specific impedances and the resulting dissipation characteristics of the liner for upstream excitation for the cases of no grazing flow (optimization step one) and no periodic bias flow (optimization step two). In both instances, the resulting dissipation is of broadband character. For the case of grazing flow, the optimized impedance is of lower resistance and the reactance exhibits an increased loss of end correction. Because of the lower resistance, the dissipation is of slightly lesser bandwidth and exhibits an increased peak value. Due to the lower reactance in the case of grazing flow, the resonance frequency is shifted slightly to higher frequencies.

Certain assumptions are made with respect to the process of optimization. Nonlinear acoustic effects due to high primary sound pressure amplitudes in the main duct are negligible under either periodic bias flow actuation or grazing flow. The former is assumed under the premise that the particle velocity $|\bar{u}_s|$ is larger than the particle velocity induced

Table 2 Parameters of the optimized facing sheet.

	$\lvert\bar{u}_{s,opt}\rvert$ [m/s]	$M_{avg,opt}$	d [mm]	h [mm]	Φ [%]
Step 1 ($M_{avg} = 0$)	14.31	–	1.62	1.04	4.94
Step 2 ($\lvert\bar{u}_s\rvert = 0$)	–	0.14	1.62	1.04	4.94

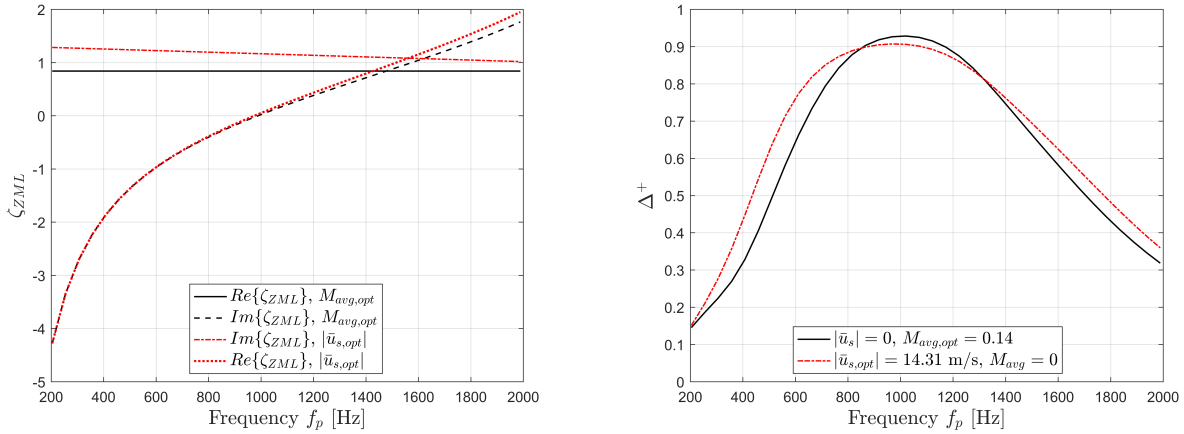

(a) Predicted specific impedance ζ_{ZML}.

(b) Predicted dissipation for upstream excitation Δ^+.

Fig. 3 Results of the optimization.

in the orifices of the facing sheet by the primary sound field [3]. The latter is verified empirically for a sound pressure level of 130 dB in the main duct. For $M_{avg} \geq 0.1$, the nonlinear acoustic effects of the primary sound field on the impedance are found to be negligible. The propagation of sound in sections 1 and 2 of the computational domain (see Fig. 5) is restricted to plane waves. Under certain circumstances, the impedance expresses a dependency on the secondary actuation frequency f_s [3]. The dependency of the impedance on f_s is neglected. The cavity back wall of the liner is assumed to be rigid, despite the attached acoustic actuator. Limiting values have been set to keep the geometric parameters of the facing sheets in the range of values, the semi-empirical model was derived in and verified for. Furthermore, achievable values must be maintained with regards to practicability. An example is the combination of the actuator particle velocity $|\bar{u}_s|$ and the porosity of the facing sheet Φ. The change of resistance due to the periodic bias flow actuation, as well as $|\bar{u}_s|$ itself, are a function of Φ (see Eqs. (5) and (22)). Hence, in order to achieve sufficiently high $|\bar{u}_s|$ and adequately increase the resistance for facing sheets of high porosity, considerable sound pressure amplitudes are necessary, that may not be achieved practically or only with great effort, respectively. Simultaneously, considering Eq. (6), the value of Φ also determines the maximum grazing flow velocity the Zero Mass Flow concept can be applied to. The limits, imposed on the optimization process, are listed in table 1.

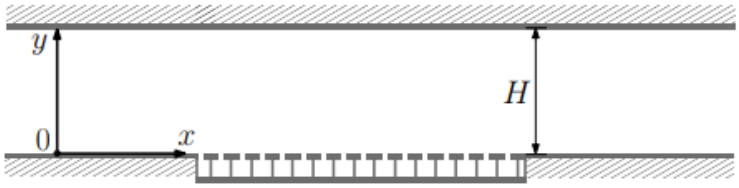

Fig. 4 Two dimensional channel with a perforated wall.

B. Numerical Method

This section outlines the numerical method utilized in the optimization. The propagation of sound under mean flow in a two dimensional channel with a section of perforated wall, similar to Fig. 4, is calculated by solving the two dimensional convected Helmholtz equation (2DCHE) for a harmonic perturbation of the acoustic pressure $\tilde{p}$. The 2DCHE is solved by means of the finite difference method. Further details of the numerical procedure can be found in Weng et al.[13]. The two dimensional convected Helmholtz equation is given by:

$$(1 - M_{avg}^2)\frac{\partial^2 \tilde{p}}{\partial x^2} + \frac{\partial^2 \tilde{p}}{\partial y^2} - 2jk_p M_{avg}\frac{\partial \tilde{p}}{\partial x} + k_p^2 \tilde{p} = 0, \tag{14}$$

where $k_p = \omega_p / c_0 = 2\pi f_p / c_0$ is the wave number. The boundary condition on the hard wall is given by:

$$\frac{\partial \tilde{p}}{\partial y} = 0. \tag{15}$$

The boundary condition on the perforated wall is given by the Ingard-Myers condition, where the specific impedance of the ZML ζ_{ZML} from Eq. (12) is applied as specific wall impedance:

$$\left[\frac{jk_p}{\zeta_{ZML}} + \frac{2M_{avg}}{\zeta_{ZML}}\frac{\partial}{\partial x} - \frac{jM_{avg}^2}{k_p \zeta_{ZML}}\frac{\partial^2}{\partial x^2}\right]\tilde{p} - \frac{\partial \tilde{p}}{\partial y} = 0. \tag{16}$$

At the inlet plane, a pressure profile is prescribed as boundary condition. Given that only plane waves propagate, the boundary condition at the exit of the numerical domain is of the form[14]:

$$\frac{jk_p \tilde{p}}{M_{avg} + \zeta_{exit}} + \frac{\partial \tilde{p}}{\partial x} = 0, \tag{17}$$

where ζ_{exit} represents the specific impedance at the exit of the numerical domain. ζ_{exit} is set to $\zeta_{exit} = 1$. In addition, an anechoic condition in form of a perfectly matched layer (PML) is imposed on the outlet plane [15, 16]. Fig. 5 displays the computational domain with an exemplary mesh for a primary frequency of $f_p = 510$ Hz. The domain is divided in three sections: Sections 1 and 3 represent the hard walled channel sections, while section 2 contains the lined segment with impedance ζ_{ZML} as the lower wall. The upper wall of section 2 is defined as hard wall respectively. Sections 1 and 3 are of length 0.9 m, while the lined section is of length 0.204 m. This corresponds to the effective

length L_{eff} of the subsequently manufactured ZML. y = 60 mm corresponds to the height above the lined surface H and is adapted from the DLR flow channel DUCT-R, which is described in Sec. V.A. The length of the PML in x-direction D is dynamic and always corresponds to half of the wave length of the frequency of the pressure perturbation that is calculated $D = 0.5\lambda_p$. 2-D Gauss-Lobatto grid points are applied in each section for the mesh generation. At the interfaces between adjacent sections the continuity of $\tilde{p}$ and $\frac{\partial \tilde{p}}{\partial x}$ is applied. The number of grid points is increased at the transitions from hard wall to lined section and vice versa. A convergence analysis is performed to determine a sufficient number of grid points. Once the pressure distribution in the channel is calculated, the pressure values at several x-coordinates in sections 1 and 3 are used to decompose the wave field into incident and reflected plane waves at the lined surface. Thermo-viscous effects are neglected in the pressure calculations but incorporated in the plane wave decomposition. Subsequently, the scattering coefficients are derived and the dissipation $\Delta^{\pm}$ for upstream and downstream excitation is calculated. The decomposition method and the calculation of the scattering coefficients and $\Delta^{\pm}$ is similar to the procedure used in the experimental evaluation, see Sec. V.B.

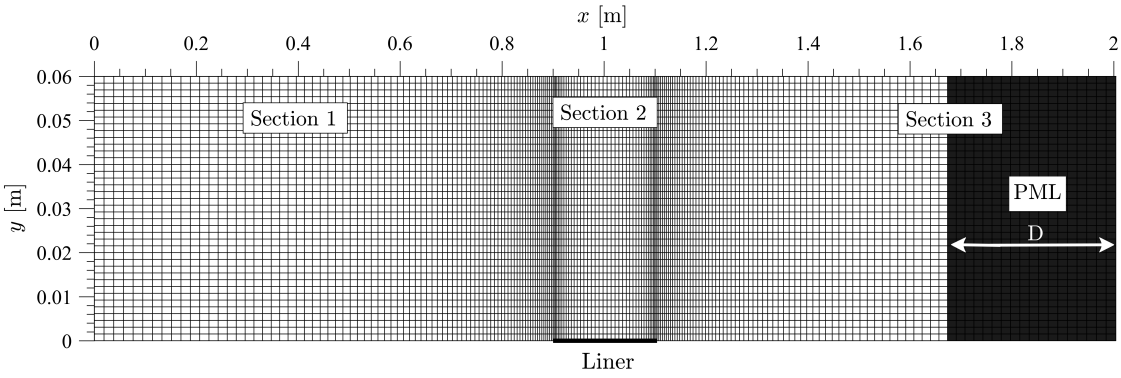

Fig. 5 Meshed computational domain.

C. Liner Design and Manufacturing

The facing sheet and the liner body are manufactured from aluminum. The liner features an overall length of 220 mm. The back wall is of thickness 7 mm and the side walls are of thickness 4 mm. The cavity is divided into three identical chambers of size 68 mm x 72 mm x 60 mm, divided by walls of thickness 4 mm. The cut-on frequency for the propagation of higher modes in each chamber is just about 2385 Hz. The effective length of the liner is approximately L_{eff} = 204 mm. Each chamber is equipped with an inlet for the induction of periodic bias flow and two chambers are equipped with several flush mounted microphones each, to allow an estimation of the induced particle velocity via a plane wave decomposition. Figs. 6 a) to d) show the CAD model of the liner body, the perforated facing sheet and the manufactured ZML, installed in DUCT-R, including cavity microphones and periodic bias flow actuators. The periodic bias flow is excited by speakers, one connected to each cavity chamber via a tubing system with a diameter of 10 mm.

Hence, the inlets are small compared to the area of the cavity back wall. Nevertheless, the inlets cause derivations from a rigid cavity by introducing additional resonances. The tubing system, connecting the speakers to the cavity chambers, is of length 250 mm. Loudspeakers serve as actuators in order to retain maximum flexibility regarding the actuation frequency. The facing sheet was manufactured by drilling with a slightly higher porosity of $\phi = 5.17$ %. This difference arises due to the fact, that the orifices have to be distributed homogeneously over the sub areas of the chambers without placing parts of the orifices above the separating walls of the chambers or reducing the effective, perforated area of the liner. The plate is screwed on the liner body on the horizontal walls as well as on the vertical walls with countersunk bolts.

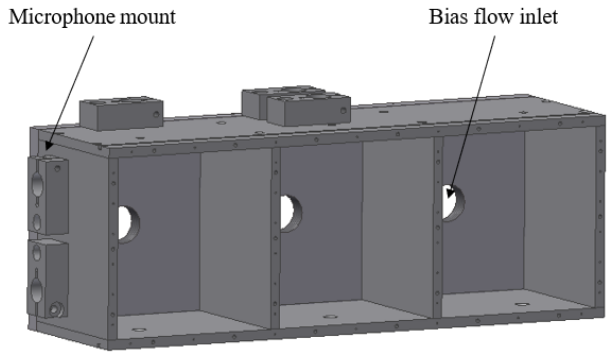

(a) CAD of ZML body.

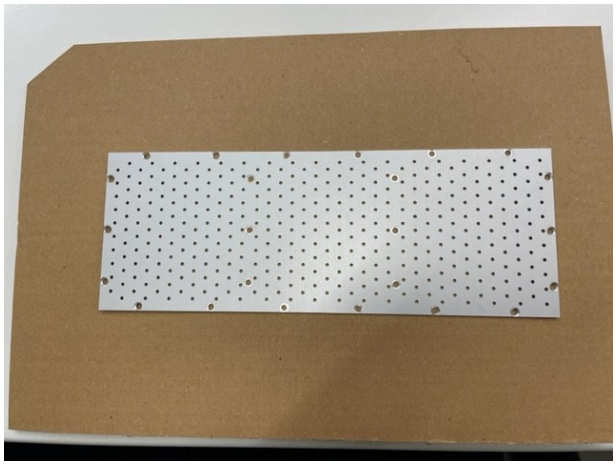

(b) Manufactured facing sheet.

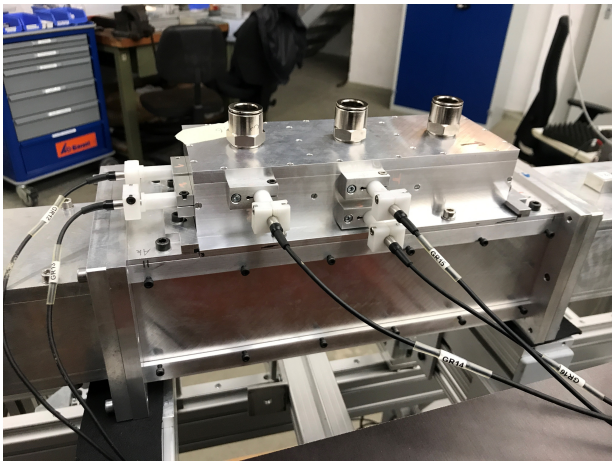

(c) ZML, with cavity microphones, installed in DLR flow duct facility DUCT-R.

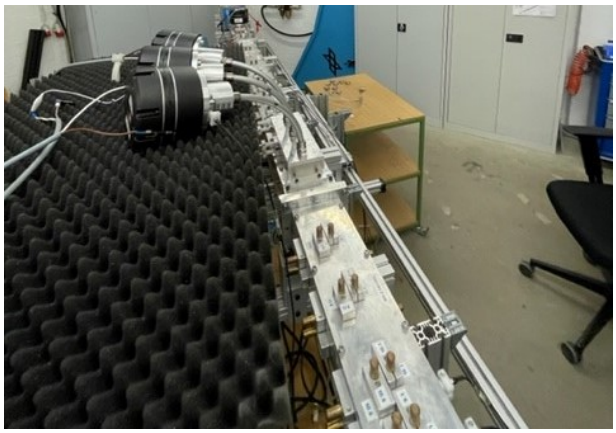

(d) Periodic bias flow actuators.

Fig. 6 Designed and manufactured ZML.

V. Experimental Setup and Analysis Method

A. Experimental Setup

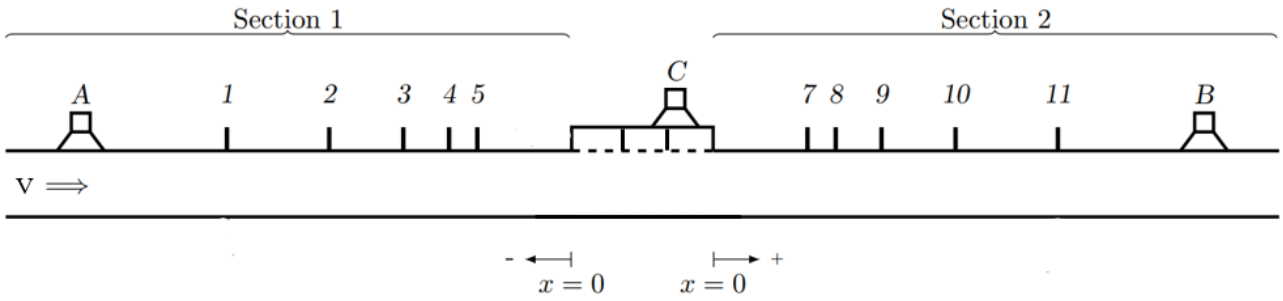

Fig. 7 Experimental Setup.

Fig. 7 depicts the experimental setup. The ZML is mounted between the two duct sections of the flow duct facility DUCT-R of the German Aerospace Center (DLR), Berlin. The rectangular duct is of width 80 mm and height 60 mm and, in the no-flow case, features plane wave excitation up to approximately 2150 Hz. Grazing flow can be applied via section 1, allowing for grazing flow speeds up to $M_{avg} \approx 0.25$. To calculate c_0, the temperature in the duct is measured by a PT100 sensor at the end of section 2. A Prandtl's tube is used to measure and monitor the center line grazing flow velocity in section 2. The measured center line velocities correspond to previous measurements of the flow profile in the hard walled sections of the duct [17]. Subsequently, the bulk grazing flow velocity v_{avg} is estimated by averaging over the respective flow profiles. Each section is equipped with an anechoic termination. The sound field in the duct is, in the form of single tone stimuli, alternately excited by loudspeakers LS A and LS B in the frequency range $204 \leq f_p \leq 1989$ Hz, allowing for a wave decomposition independent of end reflections[18]. In case of upstream excitation, utilizing LS A, the primary stimuli propagate downstream. Exciting the primary stimuli with LS B represents a downstream excitation respectively and the sound propagates in upstream direction. The sound pressure level is defined in terms of the RMS level of the plane wave incident on the measurement section at $x = 0$ and is set to $\bar{p}_i = 130$ dB for all frequencies f_p. The influence of the sound pressure level in the duct on the impedance of the ZML is found to be negligible for the case of bias flow actuation or grazing flow with $M_{avg} \geq 0.1$. Each section is equipped with five logarithmically spaced microphones to capture the sound field in the duct. The secondary stimulus for the actuation of periodic bias flow is actuated by three speakers, one for each chamber of the cavity. This is depicted in Fig. 7 as a single speaker LS C respectively. The speakers are connected to the same signal generator in parallel, so phase differences between the speakers are assumed to be small. The secondary stimulus, inducing the periodic bias flow, is a pure sine tone. Harmonics are neglected due to their minor influence compared to the fundamental[3]. During the experimental program, we found $|\bar{u}_s|$ to vary slightly between the respective chambers of the liner due to the individual transfer functions of the speakers. Furthermore, with increasing operating time, the sound pressure radiated from the speakers, actuating the secondary flow, declined slightly. Hence, additional variation of $|\bar{u}_s|$ over the measurement

points is introduced. The measurement program was conducted in intervals to limit the variations of $|\bar{u}_s|$. As primary stimuli of high sound pressure amplitudes are found to reduce the induced $|\bar{u}_s|$ [3], the location of the chambers with respect to the side of excitation in the main duct might also cause variation of $|\bar{u}_s|$ between the chambers. The primary sound waves are attenuated while propagating along the lined surface. Accordingly, the chambers located nearer to the excitation source are exposed to higher primary sound pressures than the chambers further away. Evaluation of the data shows no dependency of the variation of $|\bar{u}_s|$ over the different chambers relative to the direction of excitation. Hence, the effect is considered to be negligible for a primary sound field with $\bar{p}_i = 130$ dB. The respective values of $|\bar{u}_s|$ listed in Sec. VI represent values averaged over the chambers and measurement points. The actuation frequency of the secondary stimulus f_s is chosen in a way, that the transmission efficiency through the tubing systems is maximum and plane wave propagation is ensured. f_s is found to be $f_s = 1235$ Hz for the given setup by exciting the cavity chambers simultaneously with a sweep signal.

B. Analysis Method

The primary sound field in the duct is excited alternately with speakers LS A and LS B and the microphone data in the duct is analyzed separately in sections 1 and 2. This results in four equations for the complex sound pressure in the duct:

$$\hat{p}_{1,a}(x) = \hat{p}^{+}_{1,a} e^{-ik^{+}_{p,1}x} + \hat{p}^{-}_{1,a} e^{ik^{-}_{p,1}x}, \tag{18a}$$

$$\hat{p}_{2,a}(x) = \hat{p}^{+}_{2,a} e^{-ik^{+}_{p,2}x} + \hat{p}^{-}_{2,a} e^{ik^{-}_{p,2}x}, \tag{18b}$$

$$\hat{p}_{1,b}(x) = \hat{p}^{+}_{1,b} e^{-ik^{+}_{p,1}x} + \hat{p}^{-}_{1,b} e^{ik^{-}_{p,1}x}, \tag{18c}$$

$$\hat{p}_{2,b}(x) = \hat{p}^{+}_{2,b} e^{-ik^{+}_{p,2}x} + \hat{p}^{-}_{2,b} e^{ik^{-}_{p,2}x}. \tag{18d}$$

$\hat{p}^{+}$ and $\hat{p}^{-}$ are the complex amplitudes of the upstream and downstream propagating waves. The subscripts denote the duct section and excitation with LS A or LS B respectively. The recorded signals are transformed into the frequency domain by applying Chung's method to reject uncorrelated flow noise[19]. To derive the complex pressure amplitudes, Eqs. (18a) to (18d) are fitted to the microphone data. Thermo-viscous losses at the wall are incorporated in the wave number k_p by the solution of Dokumaci[20]. Consequently, the complex sound pressure amplitudes at $x = 0$ are identified. The sound pressure amplitudes are related to each other via the scattering coefficients r and t of the lined surface. r is the reflection coefficient, describing the reflected part of the sound wave at the transition from rigid to lined wall, and t is the transmission coefficient. Figure 8 depicts the sound field in the duct for excitation with LS A and LS B. r and t are calculated by combining both measurements and rewriting Eqs. (18a) to (18d):

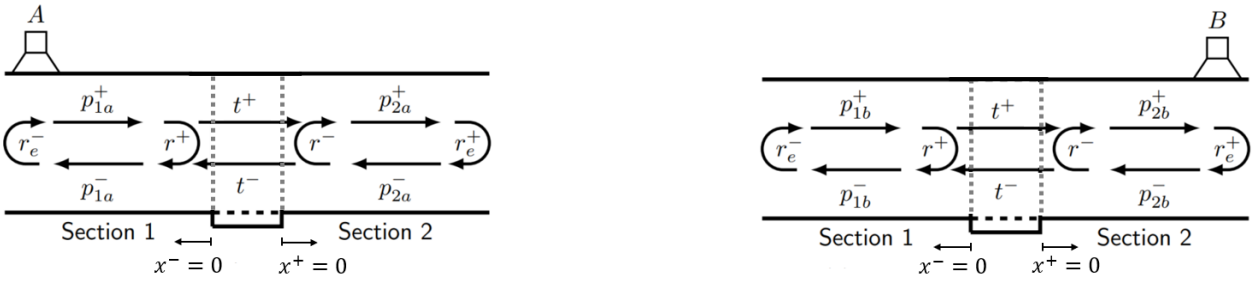

(a) Upstream excitation, measurement A.

(b) Downstream excitation, measurement B.

Fig. 8 Sound field in the duct for upstream and downstream excitation.

$$r^+ = \frac{\hat{p}_{1,a}^- \hat{p}_{2,b}^- - \hat{p}_{1,b}^- \hat{p}_{2,a}^-}{\hat{p}_{1,a}^+ \hat{p}_{2,b}^- - \hat{p}_{1,b}^+ \hat{p}_{2,a}^-}; \qquad r^- = \frac{\hat{p}_{1,a}^+ \hat{p}_{2,b}^+ - \hat{p}_{1,b}^+ \hat{p}_{2,a}^+}{\hat{p}_{1,a}^+ \hat{p}_{2,b}^- - \hat{p}_{1,b}^+ \hat{p}_{2,a}^-}; \tag{19}$$

$$t^+ = \frac{\hat{p}_{2,a}^+ \hat{p}_{2,b}^- - \hat{p}_{2,b}^+ \hat{p}_{2,a}^-}{\hat{p}_{1,a}^+ \hat{p}_{2,b}^- - \hat{p}_{1,b}^+ \hat{p}_{2,a}^-}; \qquad t^- = \frac{\hat{p}_{1,a}^+ \hat{p}_{1,b}^- - \hat{p}_{1,b}^+ \hat{p}_{1,a}^-}{\hat{p}_{1,a}^+ \hat{p}_{2,b}^- - \hat{p}_{1,b}^+ \hat{p}_{2,a}^-}. \tag{20}$$

From the scattering coefficients, the dissipation Δ is calculated. Δ is a measure of the sound energy dissipated along the lined surface. While Δ^+ represents the dissipation in case of upstream sound excitation (LS A), Δ^- represents the dissipation in case of downstream excitation (LS B).

$$\Delta^\pm = 1 - \left(\frac{(1 \mp M_{avg})^2}{(1 \pm M_{avg})^2} \cdot |r^\pm|^2 + |t^\pm|^2 \right). \tag{21}$$

To estimate $|\bar{u}_s|$, the sound field in the cavity, actuated by LS C, is also decomposed into incident and reflected waves, similar to the process described above. Note, that due to the low microphone spacing in the cavity, the plane wave decomposition should be considered an estimate. From the plane wave components in the cavity, $|\bar{u}_s|$ is calculated from Euler's equation under the assumption of continuity:

$$|\bar{u}_s| = \frac{|\hat{p}_{s,cav}^+ - \hat{p}_{s,cav}^-|}{\rho_0 c_0 \Phi \sqrt{2}}, \tag{22}$$

where $\hat{p}_{s,cav}^+$ describes the incident plane wave component at the facing sheet and $\hat{p}_{s,cav}^-$ describes the reflected component respectively.

VI. Results

A. Experimental Evaluation of the Optimization Process

Figure 9(a) depicts the measured dissipation coefficients compared to the dissipation obtained in the optimization process for the case $|\bar{u}_{s,opt}|$ and $M_{avg} = 0$. Compared to the optimized value $|\bar{u}_{s,opt}| = 14.31$ m/s, the measured

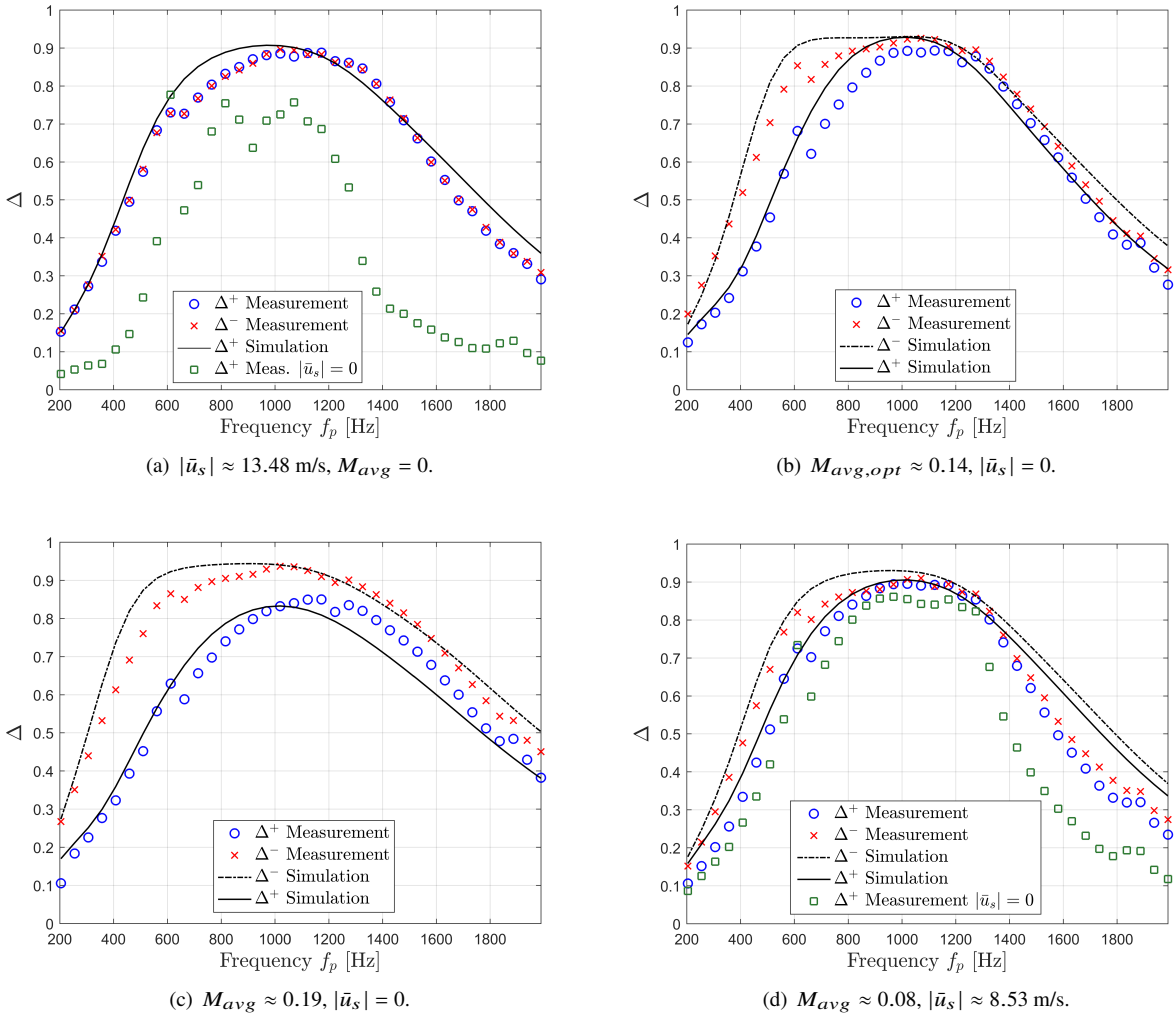

(a) $|\bar{u}_s| \approx 13.48$ m/s, $M_{avg} = 0$.

(b) $M_{avg,opt} \approx 0.14$, $|\bar{u}_s| = 0$.

(c) $M_{avg} \approx 0.19$, $|\bar{u}_s| = 0$.

(d) $M_{avg} \approx 0.08$, $|\bar{u}_s| \approx 8.53$ m/s.

Fig. 9 Measured dissipation compared to results from the optimization process.

particle velocity of the periodic bias flow, averaged over all chambers and measurement points, is $|\bar{u}_s| \approx 13.48$ m/s. The numerical simulation combined with the proposed impedance model accurately predicts the measured dissipation. Slight disagreement is found for 600 Hz $\leq f_p \leq$ 1400 Hz due to additional cavity resonances induced by the bias flow supply. These deviations are a consequence of the assumption of a rigid cavity back wall and can be observed in all measurement results. For $f_p \geq 1500$ Hz some minor disagreement is observed as well. The deviations are assumed to be connected to the previously mentioned decline of $|\bar{u}_s|$ with increasing measurement time. For 600 Hz $\leq f_p \leq$ 1400 Hz, the dissipation is larger than 0.7. The peak dissipation is approximately 0.9. To demonstrate the effect of the periodic bias flow actuation, the dissipation of the liner, without periodic bias flow actuation, is also depicted in Fig. 9(a). Without the actuation, the liner essentially acts as a SDOF liner. Compared to the case of periodic bias flow active, the dissipation is narrow-band and of lower peak value, because the resistance of the lined surface is too low. The dissipation curve

shows distinct additional resonance effects due to the periodic bias flow inlets, most prominent at $f_p \approx 600$ Hz. As the resonance effects decline with an increasing resistance, i.e. for increased periodic bias flow or grazing flow, they will not be discussed in detail.

Figure 9(b) depicts the measured dissipation coefficients for upstream and downstream excitation of the primary sound field compared to the dissipation obtained in the optimization process for the case $|\bar{u}_s| = 0$, $M_{avg,opt} = 0.14$. At $|\bar{u}_s| = 0$ and $M_{avg,opt} = 0.14$, the designed liner represents an optimized SDOF liner, with respect to the target function τ. The decrease of resistance due to the absence of the secondary actuation is retained by the grazing flow. Measurement and prediction again show favorable agreement. As expected from the results of the optimization, the dissipation expresses slightly less broadband character and a slightly higher peak value compared to the case of periodic bias flow actuation. Additionally, the results from a simulation for downstream excitation are plotted. For downstream excitation, simulation and measurement also obtain good agreement. Compared to the case of upstream excitation, the broadband character is increased further.

Figure 9(c) shows the comparison of the measured and simulated dissipation for $M_{avg} = 0.19$ and $|\bar{u}_s| = 0$. Good agreement between measurement and prediction is achieved. Compared to the case $M_{avg} = 0.14$, the broadband dissipation is increased while the peak dissipation is decreased, because of the risen resistance. For the case of upstream excitation, the resistance increased above its respective optimum, but the dissipation performance is still acceptable. For the case of downstream excitation, the obtained dissipation is of high peak and large bandwidth, emphasizing that the optimization needs to be conducted for upstream and downstream excitation separately.

For a decrease of grazing flow below its optimum value, in order to maintain a high degree of dissipation, the decrease of resistance is compensated by the actuation of periodic bias flow. Figure 9(d) displays the measured dissipation for $M_{avg} = 0.08$ and $|\bar{u}_{s,opt}| = 8.6$ m/s to the results of the simulation. Thereby, the necessary $|\bar{u}_s|$ is found by conducting the optimization for $M_{avg} = 0.08$ with fixed geometrical parameters. The measured secondary particle velocity is $|\bar{u}_s| \approx 8.53$ m/s. Compared to the case of only periodic bias flow or only grazing flow, measurement and prediction express larger discrepancies for $f_p \geq 1400$ Hz for both upstream and downstream excitation. The model overestimates the dissipation at high f_p. Furthermore, also here, the dissipation for $|\bar{u}_s| = 0$ in case of upstream excitation is depicted. At $|\bar{u}_s| = 0$, the dissipation is of more narrow band character, because the resistance of the lined surface is still comparably low. By applying the periodic bias flow, the resistance is increased and the liner is tuned towards a broadened dissipation bandwidth.

B. Combined Periodic Bias and Grazing Flow

The grazing flow is found to suppress the periodic flow through the orifice. Consequently, the amplitude of the periodic bias flow is reduced with increasing grazing flow speeds. This is similar to the effect of a high amplitude primary sound field on the periodic bias flow [3]. Fig. 10(a) to 10(c) compare the measured dissipation for various

grazing flow conditions with and without periodic bias flow actuation. Thereby, the ratio $\frac{v_{avg}}{|\bar{u}_s|}$, where v_{avg} is the average grazing flow speed, is increased from $\frac{v_{avg}}{|\bar{u}_s|} \approx 2.23$ to $\frac{v_{avg}}{|\bar{u}_s|} \approx 8.99$. For a ratio of $\frac{v_{avg}}{|\bar{u}_s|} \approx 2.23$ ($M_{avg} \approx 0.08$, $|\bar{u}_s| \approx 12.27$ m/s), the effect of the secondary actuation is clearly visible. Increasing $\frac{v_{avg}}{|\bar{u}_s|}$ leads to a reduced effect of the periodic bias flow. For $\frac{v_{avg}}{|\bar{u}_s|} \approx 5.1$ ($M_{avg} \approx 0.14$, $|\bar{u}_s| \approx 9.33$ m/s), the effect of the periodic bias flow on the dissipation is reduced considerably. For $\frac{v_{avg}}{|\bar{u}_s|} \approx 8.99$ ($M_{avg,max} = 0.19$, $|\bar{u}_s| \approx 7.3$ m/s), only a minor effect due to periodic bias flow around the resonance frequency of the liner is obtained. Thus, we assume the impedance of the lined surface is only negligibly affected by the periodic bias flow. The effect of high sound pressure levels on orifices and lined surfaces in grazing flows has been studied previously [21–23]. Thereby, the skin friction velocity v^* is compared to the peak amplitude of the acoustic particle velocity in the orifice $|u_0|$. As soon as v^* is in the order of the acoustic particle velocity in the orifices, the impedance change due to the high acoustic amplitudes is reduced. Goldman and Panton [21] for example, compare v^*, measured on a rigid wall part of the duct, to $|u_0|$ and find that effects due to high sound pressure amplitudes on the impedance of orifices are found only for $\frac{|u_0|}{v^*} > 3$. While determining v^* is out of scope of this study, previously measured data from the measurement facility is used for a comparison [17]. For $M_{avg} = 0.2$, v^* is found to be $v^* \approx 2.74$. Hence, the case $\frac{v_{avg}}{|\bar{u}_s|} \approx 8.99$ corresponds to $\frac{\sqrt{2}|\bar{u}_s|}{v^*} \approx 3.77$, agreeing to the values found in the literature.

C. Discussion of the Results

The results demonstrate, that compared to a single degree of freedom liner, a high degree of dissipation is obtained over a range of grazing flow velocities by the appropriate adjustment of the velocity of the secondary periodic bias flow. Furthermore it is shown, that the optimization routine can be used in the design of acoustic liners. The predicted dissipation of the Zero Mass Flow Liner, derived from the proposed impedance model in combination with the optimization method, agrees to the measurement results. Since the cavity was modeled under the assumption of a rigid back wall, minor deviations between prediction and measured dissipation arise due to additional cavity resonances introduced by the bias flow inlets. The accuracy of the impedance model of the Zero Mass Flow Liner can be increased by incorporating the actual impedance of the cavity. Dependent on the properties of the actuation supply, the impedance of the cavity might be difficult to derive analytically and needs to be measured beforehand. Therefore, a rigid cavity back wall was assumed in the process. The designed Zero Mass Flow Liner obtains broadband dissipation of high peak level for a grazing flow regime of $0 \leq M_{avg} \leq 0.2$ by inducing flow separation at the facing sheet of the liner and actively affecting its impedance. Utilizing multiple cavities of different depths, a high degree of broadband damping could be achieved. In principle, a liner can be designed to function over a range of desired grazing flow speeds. The liner should be designed in a way that, at the highest flow speed of consideration, no periodic bias flow is necessary. The decrease of resistance with decreasing grazing flow Mach number at differing operating conditions, can be compensated by applying the periodic bias flow actuation. With increasing grazing flow speeds however, the effect of the periodic bias flow gets suppressed. For high Mach numbers, a considerable amount of energy is necessary to achieve the desired

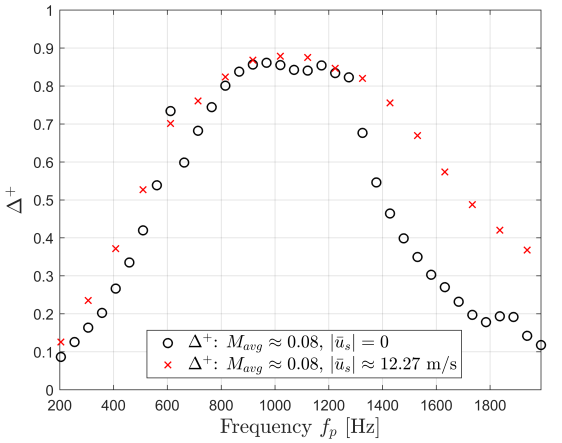

(a) $\frac{v_{avg}}{|\bar{u}_s|} \approx 2.23$.

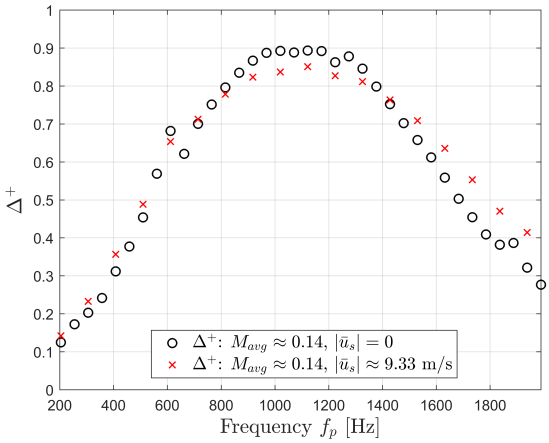

(b) $\frac{v_{avg}}{|\bar{u}_s|} \approx 5.1$.

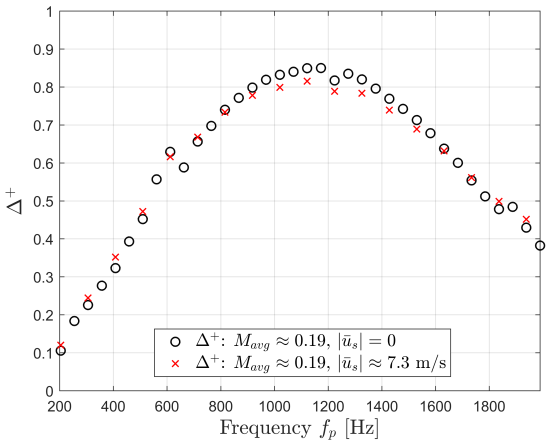

(c) $\frac{v_{avg}}{|\bar{u}_s|} \approx 8.99$.

Fig. 10 The effect of periodic bias flow with increasing grazing flow speed.

effect. For a ratio of grazing flow to periodic bias velocity of approximately $\frac{v_{avg}}{|\bar{u}_s|} > 5$, no appreciable effect of the periodic bias flow actuation on the dissipation characteristics of the liner is found. Consequently, the applicability of the concept under grazing flow is strongly dependent on the power of the secondary actuation source. For example, utilizing the Zero Mass Flow concept for grazing flows with $M_{avg} = 0.3$, a periodic bias flow velocity of $|\bar{u}_s| > 20.6$ m/s needs to be applied, to achieve an effect and increase the resistance. For $M_{avg} = 0.5$, a secondary velocity of $|\bar{u}_s| > 34.3$ m/s is already required. This poses a high energy requirement on the actuation source, especially, when considering the high porosity necessary in the design of facing sheets for liners at high grazing flow velocities. While leakage of the bias flow actuation into the duct is not considered in this study, negative effects on the damping performance are expected and a trade-off analysis between the additionally induced noise and the enhanced damping needs to be conducted. Therefore, the actuation frequency should be preferably chosen in a way, that the propagation in the main duct is minimized. Taking

into account all effects and tuning the components of the system properly, constitutes a challenge to the liner design.

VII. Conclusion and Outlook

In this study, the Zero Mass Flow concept is evaluated in a flow duct for grazing flow velocities up to a Mach number of 0.2. The concept utilizes periodic bias flow, induced by means of acoustic actuation, to enhance the damping capabilities of lined surfaces over various grazing flow conditions. Thereby, the amplitude of the periodic bias flow is adapted to keep the resistance of the lined surface in a value range, where high damping is ensured. An impedance model, accounting for the effects of periodic bias flow and grazing flow, is proposed and an optimization routine for the design of liners is described. Utilizing the optimization method, a Zero Mass Flow Liner is manufactured. Consequently, the damping characteristics of the liner are evaluated experimentally for single tone stimuli with amplitudes of 130 dB. The derived optimization process proves to be a viable tool in the design of acoustic liners. The predicted damping characteristics show reasonable agreement to the measurements. The Zero Mass Flow concept obtains broadband dissipation over a comparably large frequency range and various grazing flow velocities. For combined periodic bias flow and grazing flow, the periodic bias flow is suppressed. For a ratio of grazing flow to periodic bias flow velocity larger than approximately five, no significant effect of the periodic bias flow on the damping characteristics is observed. This might pose a problem in the realization of Zero Mass Flow Liners for high Mach number grazing flows, since a large amount of energy is necessary for the periodic bias flow actuation, in order to achieve an effect. Hence, periodic bias flow can be used to approximate the desired resistance values in low Mach number regimes, while the liner should be optimized to working without periodic bias flow at high Mach numbers. Further research regarding the interaction of periodic bias flow and grazing flow needs to be conducted to gain further insights and refine the proposed model. The Zero Mass Flow concept might especially be useful in combination with multi cavity depth liners.

Appendix

A. The Resistance of Perforated Plates under Secondary High Amplitude Excitation

The periodic bias flow Strouhal number defined as $St_{p,d} = \frac{2\pi f_p d}{|\bar{u}_s|}$ is used as criterion to differentiate between the quasi-steady flow domain and the linear impedance regime. f_p represents the frequency of a primary excitation and d the diameter of the orifices. The primary excitation can be interpreted as the sound field to be damped by the ZML. $|\bar{u}_s|$ denotes the root mean squared (RMS) secondary particle velocity in the orifices of the facing sheet. $|\bar{u}_s|$ is induced by the acoustic actuator in the cavity of the liner causing the periodic bias flow through the perforations of the facing sheet. For small Strouhal numbers $St_{p,d} < 1$, the convective contributions to the resistance are large compared to the viscous effects and the change of the specific resistance at a frequency f_p of perforated plates due to secondary high amplitude excitation $Re\{\Delta\zeta_s\}$ can be approximated by using a quasi-steady assumption [3]:

$$Re\{\Delta\zeta_s\} = \frac{(1-\Phi^2)|\bar{u}_s|}{2c_0\Phi C_{d,nl}^2}, \tag{23}$$

where $C_{d,nl}$ describes the discharge coefficient approximated empirically, Φ represents the porosity of the facing sheet and c_0 describes the speed of sound in air. Conversely, for large Strouhal numbers $St_{p,d} \gg 1$ the convective contributions to the impedance can be neglected. Hence, the viscous contributions dominate and the impedance is only dependent on its geometric specifications. This regime is referred to as linear regime. Applying the quasi-steady approximation in the transitional domain between linear and quasi-steady flow regime may result in significant errors, when modelling the impedance of perforated plates. Temiz et al. [24] extensively treated the impedance of micro-perforated plates in the transmission regime for single tone excitation. An empirical approximation to assess the effects of a secondary actuation on the resistance of perforated plates in transmission regime can be derived by analyzing the difference between the quasi-steady approximation and the measured resistance. The derivation is based on measurements of the impedance of perforated plates [3, 4], where the experimental setup and the evaluation method are described as well. We assume, that the change of resistance of the perforated sheet in the transitional domain can be approximated by Eq. (23) multiplied with an empirical factor Υ.

$$Re\{\Delta\zeta_s\} = \frac{(1-\Phi^2)|\bar{u}_s|}{2c_0\Phi C_{d,nl}^2} \cdot \Upsilon, \tag{24}$$

To obtain the deviation from the quasi-steady model, i.e. Υ, we divide the measured resistance values by Eq. (23) and yield:

$$\Upsilon = \frac{Re\{\Delta Z_s\} \cdot C_{d,nl}^2 \cdot 2\Phi}{(1-\Phi^2)\rho_0|\bar{u}_s|}, \tag{25}$$

where $Re\{\Delta Z_s\} = Re\{\Delta\zeta_s\} \cdot \rho_0 c_0$. Fig. 11 (a) and (b) show Υ, for two perforated plates, plotted against the inverse Strouhal number $1/St_{p,d}$. The dashed line represents the quasi-steady limit. As can be seen, with increasing $1/St_{p,d} > 1$, the change of resistance approaches Eq (23). For $1/St_{p,d} \leq 1$ considerable deviations from the quasi-steady approach are observed, that approximately follow the function $\Upsilon \approx 1 - \frac{f_p d}{|\bar{u}_s|}$, depicted as the dotted line. For the perforate depicted in Fig. 11 (a), a significantly different behavior of the resistance for $f_p << f_s$ (+ symbols) is observed and the impedance expresses a dependency on f_s. The deviate behavior is further discussed in Burgmayer et al. [3]. For high $|\bar{u}_s|$, Υ approaches 1. For low $|\bar{u}_s|$, high f_p and large d, Υ can become negative as $\frac{f_p d}{|\bar{u}_s|} > 1$. Therefore, if $\Upsilon < 0$, we assume, that the resistance is independent of the particle velocity and $Re\{\Delta\zeta_s\} = 0$. The value of $\frac{f_p d}{|\bar{u}_s|} = 1$ corresponds to $1/St_{p,d} = \frac{1}{2\pi} \approx 0.16$, where effects due to high sound pressure amplitudes are negligible. Consequently, the semi-empirical model to account for the change of resistance at a primary frequency f_p due to the secondary high amplitude actuation is written as:

$$Re\{\Delta\zeta_s\} = \begin{cases} \frac{(1-\Phi^2)|\bar{u}_s|}{2c_0\Phi C_{d,nl}^2} \cdot \left(1 - \frac{f_p d}{|\bar{u}_s|}\right) & \text{for } 1/St_{p,d} \geq \frac{1}{2\pi} \\ 0 & \text{for } 1/St_{p,d} < \frac{1}{2\pi}. \end{cases} \tag{26}$$

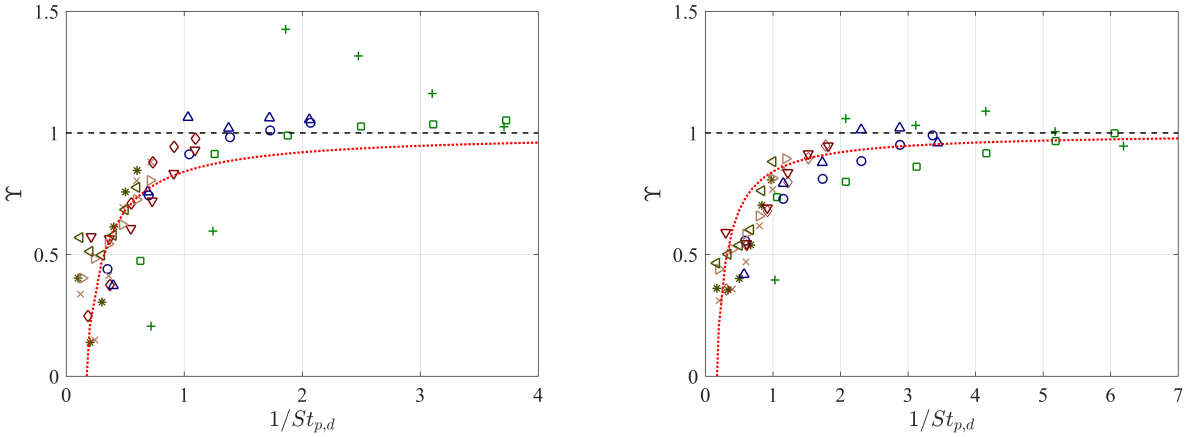

(a) Φ = 4.09 %, d = 2.5 mm, h = 1 mm.

(b) Φ = 6.18 %, d = 1.5 mm, h = 1 mm.

Fig. 11 Deviation of resistance from quasi-steady solution in the transmission regime plotted against $1/St_{p,d}$. −−: Quasi-steady solution; · · ·: Approximation of the resistance in the transmission domain. Symbol reference for the measured resistance values:

	□	+	○	△	◇	▽	x	▷	∗	◁
f_p [Hz]	255	255	459	459	867	867	1326	1326	1581	1581
f_s [Hz]	331	943	331	943	331	943	331	943	331	943

Acknowledgements

This study is supported by the project ARTEM (Aircraft noise Reduction Technologies and related Environmental iMpact) which has received funding from the European Union's Horizon 2020 research and innovation programme under Grant No. 769 350.

References

[1] Heuwinkel, C., Enghardt, L., and Röhle, I., "Concept and Experimental Investigation of a Zero Mass Flow Liner," *14th AIAA/CEAS Aeroacoustics Conference (29th AIAA Aeroacoustics Conference)*, AIAA-2008-2931, 2008. https://doi.org/10.2514/6.2008-2931.

[2] Lahiri, C., Pardowitz, B., Bake, F., and Enghardt, L., "The Application of an Aeroacoustic Actuator in a Zero Mass Flow Liner

for Acoustic Damping," *17th AIAA/CEAS Aeroacoustics Conference (32nd AIAA Aeroacoustics Conference)*, AIAA-2011-2725, 2011. https://doi.org/10.2514/6.2011-2725.

[3] Burgmayer, R., Bake, F., and Enghardt, L., "Effects of a secondary high amplitude stimulus on the impedance of perforated plates," *The Journal of the Acoustical Society of America*, Vol. 149, 2021, pp. 3406–3415. https://doi.org/10.1121/10.0004951.

[4] Burgmayer, R., Bake, F., and Enghardt, L., "Reduction of inertial end correction of perforated plates due to secondary high amplitude stimuli," *JASA Express Letters*, Vol. 2, No. 4, 2022, p. 042801. https://doi.org/10.1121/10.0009920.

[5] Atalla, N., and Sgard, F., "Modeling of perforated plates and screens using rigid frame porous models," *Journal of Sound and Vibration*, 2007, pp. 195–208. https://doi.org/10.1016/j.jsv.2007.01.012.

[6] Guess, A., "Calculation of perforated plate liner parameters from specified acoustic resistance and reactance," *Journal of Sound and Vibration*, Vol. 40, No. 1, 1975, pp. 119–137. https://doi.org/10.1121/1.1978205.

[7] Goldberg, D. E., *Genetic Algorithms in Search, Optimization and Machine Learning*, 1st ed., Addison-Wesley Longman Publishing Co., Inc., USA, 1989.

[8] Ingard, U., and Labate, S., "Acoustic Circulation Effects and the Nonlinear Impedance of Orifices," *Journal of the Acoustical Society of America*, Vol. 22, 1950, pp. 211–218.

[9] Feder, E., and Dean, L. W., "Analytical and experimental studies for predicting noise attenuation in acoustically treated ducts for turbofan engines," *NASA CR-1373*, September 1969.

[10] Ingard, U., "Absorption Characteristics of Nonlinear Acoustic Resonators," *The Journal of the Acoustical Society of America*, Vol. 44, No. 4, 1968, pp. 1155–1156. https://doi.org/10.1121/1.1911215.

[11] Laly, Z., Atalla, N., and Meslioui, S.-A., "Acoustical modeling of micro-perforated panel at high sound pressure levels using equivalent fluid approach," *Journal of Sound Vibration*, 2018, pp. 134–158. https://doi.org/10.1016/j.jsv.2017.09.011.

[12] Fok, V. A., "Theoretical study of the conductance of a circular hole, in a partition across a tube," *Proceedings of the USSR Academy of Sciences*, Vol. 31, 1941, pp. 875–878.

[13] Weng, C., Schulz, A., Ronneberger, D., Enghardt, L., and Bake, F., "Flow and Viscous Effects on Impedance Eduction," *AIAA Journal*, Vol. 56, No. 3, 2018, pp. 1118–113. https://doi.org/10.2514/1.J055838.

[14] Jones, M., Watson, W., and Parrott, T., *Benchmark Data for Evaluation of Aeroacoustic Propagation Codes with Grazing Flow*, 2005. https://doi.org/10.2514/6.2005-2853.

[15] Teixeira, F., and Chew, W., "A general approach to extend Berenger's absorbing boundary condition to anisotropic and dispersive media," *IEEE Transactions on Antennas and Propagation*, Vol. 46, No. 9, 1998, pp. 1386–1387. https://doi.org/10.1109/8.719984.

[16] Oskooi, A. F., Zhang, L., Avniel, Y., and Johnson, S. G., "The failure of perfectly matched layers, and towards their redemption by adiabatic absorbers," *Opt. Express*, Vol. 16, No. 15, 2008, pp. 11376–11392. https://doi.org/10.1364/OE.16.011376.

[17] Schulz, A., Weng, C., Bake, F., Enghardt, L., and Ronneberger, D., *Modeling of liner impedance with grazing shear flow using a new momentum transfer boundary condition*, AIAA 2017-3377, 2017. https://doi.org/10.2514/6.2017-3377.

[18] Lahiri, C., "Acoustic performance of bias flow liners in gas turbine combustors," Ph.D. thesis, Technical University Berlin, Berlin, Germany, 2013.

[19] Chung, J. Y., "Rejection of flow noise using a coherence function method," *The Journal of the Acoustical Society of America*, Vol. 62, No. 2, 1977, pp. 388–395. https://doi.org/10.1121/1.381537.

[20] Dokumaci, E., "A note on transmission of sound in a wide pipe with mean flow and viscothermal attenuation," *Journal of Sound and Vibration*, Vol. 208, 1997, pp. 653–655. https://doi.org/10.1006/jsvi.1997.1043.

[21] Goldman, A. L., and Panton, R. L., "Measurement of the acoustic impedance of an orifice under a turbulent boundary layer," *The Journal of the Acoustical Society of America*, Vol. 60, No. 6, 1976, pp. 1397–1405. https://doi.org/10.1121/1.381233.

[22] Kooi, J., and Sarin, S., *An experimental study of the acoustic impedance of Helmholtz resonator arrays under a turbulent boundary layer*, AIAA 1981-1998, 1981. https://doi.org/10.2514/6.1981-1998.

[23] Malmary, C., Carbonne, S., Auregan, Y., and Pagneux, V., *Acoustic impedance measurement with grazing flow*, AIAA 2001-2193, 2001. https://doi.org/10.2514/6.2001-2193.

[24] Temiz, M. A., Tournadre, J., Arteaga, I. L., and Hirschberg, A., "Non-linear acoustic transfer impedance of micro-perforated plates with circular orifices," *Journal of Sound and Vibration*, 2016, pp. 418–428. https://doi.org/10.1016/j.jsv.2015.12.022.